Parameter transferability, self-doping, and metallicity in LaNiO_{3}/LaMnO_{3} superlattices

Alejandro Lopez-Bezanilla, Louis-François Arsenault, Anand Bhattacharya, Peter B. Littlewood, and Andrew J. Millis

Phys. Rev. B **99**, 035133 — Published 17 January 2019

DOI: 10.1103/PhysRevB.99.035133

Parameter transferability, self-doping, and metallicity in $LaNiO_3/LaMnO_3$ superlattices

Alejandro Lopez-Bezanilla[1,2,*] Louis-François Arsenault[3], Anand Bhattacharya[2], Peter B. Littlewood[2,4], and Andrew J. Millis[3]
[1] *Theoretical Division, Los Alamos National Laboratory, Los Alamos, New Mexico 87545, United States*
[2] *Materials Science Division, Argonne National Laboratory, Lemont, Illinois 60439, USA*
[3] *Department of Physics, Columbia University, New York, New York 10027, USA and*
[4] *James Franck Institute, University of Chicago, Chicago, Illinois 60637, United States*

Motivated by recent experiments, we use the $+U$ extension of the generalized gradient approximation to density functional theory to study superlattices composed of alternating layers of $LaNiO_3$ and $LaMnO_3$. For comparison we also study a rocksalt ((111) double perovskite) structure and bulk $LaNiO_3$ and $LaMnO_3$. A Wannier function analysis indicates that band parameters are transferable from bulk to superlattice situations with the exception of the transition metal d-level energy, which has a contribution from the change in d-shell occupancy. The charge transfer from Mn to Ni is found to be moderate in the superlattice, indicating metallic behavior, in contrast to the insulating behavior found in recent experiments, while the rocksalt structure is found to be insulating with a large Mn-Ni charge transfer. We suggest a high density of cation antisite defects may account for the insulating behavior experimentally observed in short-period superlattices.

I. INTRODUCTION

The sensitive dependence of correlated electron properties on electron concentration and crystal structure has motivated the exploration of new systems that provide access to different regimes of the structure/concentration phase space. Oxide superlattices involving components with correlated electron properties are of particular interest because they present the possibility of controlled synthesis of correlated materials with specifically designed properties.[1] Efficient exploitation of the new materials fabrication capabilities to establish a broadly effective "materials by design" capability will be enhanced by the development and validation of theoretical methods and physical/chemical understanding of the relation between structure and correlated electron properties. Improved understanding of "transferability" – the extent to which parameters established by study of simpler system may be carried over to the description of a second, more complicated, situation–is important to this process, because to the extent that parameters are transferrable, intuition obtained from studies of model system and simple bulk compounds can be used to guide synthesis and *ab initio* studies of complex structures.

In this paper we address the validation and transferability issues in the context of combinations of perovskite manganite ($LaMnO_3$ or LMO) and nickelate ($LaNiO_3$ or LNO) materials into superlattices. Individually these transition-metal oxide based materials exhibit remarkable physical properties related to the interplay of magnetic, charge, orbital, and structural degrees of freedom, including colossal magnetoresistance, metal-insulator transitions and orbital and spin-ordered states[2]. Chemical doping, pressure and magnetic and electric fields have been employed to tune manganites and nickelates from one phase to another[3–5]. Gibert et. al,[6], Piamonteze and co–workers[7] and Hoffman et al[8] have studied interfaces between LNO and LMO experimentally. Gibert and co-workers[6] presented some density functional plus U studies of magnetic moments in (111) superlattices and Lee and Han[9] studied charge transfer and magnetism. In related work, Zhong, Zhang and Held[10] performed a MLWF analysis of $SrVO_3/SrTiO_3$ superlattices with the aim of constructing a model Hamiltonian to interpret the results of Yoshimatsu et al[11,12]. These authors did not address the issues of parameter transferability. Our study builds on these works, presenting new results related to parameter transferability and the physics of electron transfer in superlattices.

The present work is specifically motivated by results of Hoffman et al[13], who fabricated superlattices of the chemical formula $(LaNiO_3)_n(LaMnO_3)_n$ and showed transport and optical evidence of a metal-insulator transition occurring as n was decreased from 3 to 2. These authors further used X-ray spectroscopy to show a thickness-dependent transfer of electrons from Mn to Ni. Specifically, for a $(LNO)_2/(LMO)_2$ superlattice the cations exhibit spectra consistent with Mn^{4+} and Ni^{2+} oxidation states, very different from the nominal Mn^{3+} and Ni^{3+} oxidation states observed in the corresponding bulk materials, and associated the electron transfer with the insulating behavior.

In this paper we report results of density functional theory and density functional theory plus U (DFT+U) calculations performed to help understand the behavior of these materials and transition metal oxides more generally. While DFT+U is a mean field method that does not capture the full complexity of correlated electron materials, it does provide reasonable estimates of basic physics such as charge transfer, allows for structural relaxation, and permits a detailed analysis of parameter transferability. We consider superlattices similar to those studied experimentally and for comparison also present results for the cubic ABO_3 perovskite and

the rocksalt $A_2BB'O_6$ ((111) double pervoskite. We deal with idealized situations to get a sense of parameters and transferability and comment on the consequences of including more realistic details of the crystal structure. Maximally localized Wannier functions (MLWFs)[14] are employed to fit the band structures of the bulk compounds to tight-binding models which parametrize the Hamiltonian description of each compound. Comparison of parameters obtained from the Wannier fits indicates that the on-site energy and intersite hopping parameters are transferable (meaning that they take the same value as in the bulk parent compounds), with one exception: the transition metal electronegativity is not transferable, but instead depends on the degree of charge transfer. A related point was very recently made by Zhong and Hansmann[15] who introduced a model involving a combination of alignement of oxygen states and charge transfer. We discuss the relation of this work to ours in more detail below. These results indicate that insights from bulk materials can to a very large degree be carried over to the superlattice situation (making appropriate allowance for superlattice-induced changes in structure), but underscore the importance of an improved understanding of charge transfer and of the on-site energetics of the transition metal ions.

Our results have implications for the interpretation of the experiments of Hoffman et al[13]. In the layered situation the calculated charge transfer is much less than the one electron per Mn found experimentally, even after accounting for possible lattice relaxation; however the charge transfer found for the rocksalt structure is closer to the experimental value, suggesting that the structures fabricated by Hoffman et al have a high concentration of transition metal antisite defects, as predicted by previous work,[16] so that the actual experimental situation may correspond more closely to the rocksalt structure.

The rest of this paper is organized as follows. Section II presents the systems to be investigated and outlines the basic physics, section III presents the model and calculational methods. Section IV the energy bands that are the basic result. Section V presents an interpretation of the results. Section VII is a summary and conclusion.

II. MODEL

The systems studied are shown in Fig. 1. We consider the ideal cubic perovskite version of the bulk "parent compounds" $LaNiO_3$ and $LaMnO_3$ (panels (a) and (b)), a slightly idealized version of the superlattices studied experimentally (panel (c) of Fig. 1), and a rocksalt (111 double perovskite) structure with interpenetrating Mn and Ni sublattices (panel (d) of Fig. 1). For most of our calculations we idealize the structures to minimize the number of parameters describing the electronic physics, thus enabling a straightforward interpretation of the computations.

We begin by describing the bulk "parent compounds"

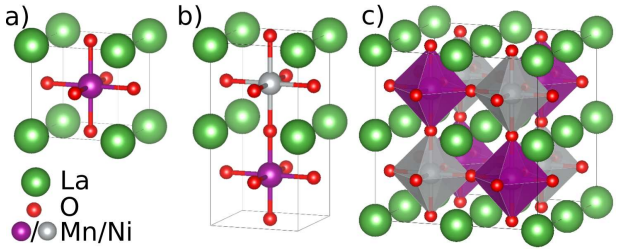

FIG. 1. Model representation of the structures studied in this paper. a) cubic $LaNiO_3$ or $LaMnO_3$, b) multilayer of $[LaMnO_3]_1/[LaNiO_3]_1$, and c) rocksalt structure of $LaMnO_3$ and $LaNiO_3$. In panel (c) where the octahedra represents the six-fold coordination of the metallic cations.

$LaNiO_3$ and $LaMnO_3$. $LaNiO_3$ (Figure 1a) is the only one of the rare earth nickelate perovskites that remains metallic and non-magnetic down to the lowest temperatures (substituting another rare earth for La produces materials that have a low temperature insulating phase characterized by a two-sublattice breathing distortion and by antiferromagnetism). $LaNiO_3$ forms in a slightly distorted version of the ideal ABO_3 perovskite structure, characterized by $R\bar{3}c$ symmetry and a pseudocubic lattice parameter of 3.83 Å. Here we approximate the structure as the simple cubic ABO_3 perovskite. Because we wish to compare to films grown on $SrTiO_3$ substrates we will choose the lattice constant to be equal to the $SrTiO_3$ pseudocubic lattice constant 3.95 Å. The relevant electronic states in $LaNiO_3$ are antibonding combinations of Ni-d and O $2p\sigma$ orbitals. From the formal valence point of view, the Ni configuration is d^7 (t_{2g}^6-e_g^1) making the material a representative spin-1/2, orbitally degenerate material. However the highest-lying oxygen states are in fact believed to lie slightly higher in energy than the Ni e_g levels, placing the material in the "negative charge transfer" class of materials[17–20] so that the actual electronic configuration is closer to $d^8\bar{L}$, with Ni in the high-spin (t_{2g}^6-e_g^2) state and one hole on the oxygen (ligand) network.

Bulk $LaMnO_3$ is an antiferromagnetic insulator. Formal valence and Hund's coupling arguments indicate the Mn configuration is high-spin d^4 with half-filled fully spin polarized t_{2g}-symmetry orbitals contributing an electrically inert $S = 1$ "core spin" and the quarter filled e_g manifold adding a potentially mobile $s = 1/2$ carrier whose spin is strongly aligned to the core spin[2,21,22] . In bulk $LaMnO_3$,[23,24] Jahn-Teller distortions involving alternating Mn-O bond lengths and $GdFeO_3$-type checkerboard tilting of the oxygen octahedra lift the orbital degeneracy of the e_g manifold, leading to an insulating ground state. Hole doping of $LaMnO_3$ reduces the tendency to Jahn-Teller order and the fully hole-doped end member $SrMnO_3$ is a cubic perovskite. Because we are interested situations in which charge transfer occurs, and because the Jahn-Teller ordering is in many cases suppressed in manganite films[25], we study the cubic symmetry crystal structure (Figure 1a); again for comparison to

films we use the bulk $SrTiO_3$ lattice constant of 3.95Å.

III. METHOD

A layered $(LaNiO_3)_n/(LaMnO_3)_n$ heterostructure may be formed by the periodic stacking of n two-dimensional layers of both $LaNiO_3$ and $LaMnO_3$ in the ideal perovskite (001) direction. Figure 1b shows the $n = 1$ case, which we focus on in this paper for simplicity of interpretation. We note that this structure should show maximal charge transfer effects. To account for the strain induced by the substrate on which the experimental heterostructures were grown, the in-plane lattice parameters are fixed to the calculated bulk $SrTiO_3$ lattice constant of 3.95 and the out of plane lattice parameter to 2× 3.95Å. Rotation of the transition metal-oxygen octahedra was not allowed. We considered three cases for internal coordinates: the apical O atoms at the same distance between the Mn and the Ni atoms, and displaced 0.2 and 0.4 Å towards the Mn.

Finally we studied a $A_2BB'O_6$ double perovskite (rocksalt) structure (Figure 1c) in which the six nearest cations to each Mn are Ni and conversely. The Mn-Ni distance was again taken to be equal to the $SrTiO_3$ pseudocubic lattice constant of 3.95Å. This structure is chosen to provide extra insight into the dependence of charge transfer on structure and also serves as a computationally tractable proxy for a superlattice with a very high density of cation antisite defects.

We use the density functional +U (DFT+U) method, in which density functional band calculations are supplemented with on-site interactions among the transition metal d-orbitals. While DFT+U is a mean field method that does not fully capture the complexities of correlated electron physics, it does adequately represent the basic energetics of materials, in particular capturing correctly the basic energetics associated with charge transfer. An important issue in this method is the choice of interaction parameters U and J and the corresponding double counting correction. According to previously reported results[26], an on-site intra-d interaction term U_{Mn}=4 eV and J_{Mn}=1.0eV, provides an adequate description of $LaMnO_3$, successfully separating the higher-lying local minority spin t_{2g} states from the local majority e_g bands above a band gap which is likewise increased. When used with the experimental low temperature *Pbnm* structure this U_{Mn} produces results consistent with experiment. The on-site interaction term for Ni has been chosen to U_{Ni}=6.0 eV J_{Ni}=1.0 eV comparable to values used in the literature[27].

The fully localized limit (FLL) double-counting correction was employed. This double counting correction in effect compensates the Hartree shift of the transition metal d orbital, fixing the relative electronegativities of the transition metal and oxygen orbitals at about the values found in the density functional calculations.

The spin-polarized DFT calculations were performed using the projector augmented-wave method[28] and the PBE-GGA exchange-correlation functional[29] with +U corrections in the Dudarev et al. scheme[30] as implemented in the VASP code[31–33]. The rotationally invariant method with an effective $U_{eff} = U - J$ was employed. The electronic wave-functions were described using a plane-wave basis set with an energy cutoff of 500 eV. Atomic positions were fixed in the cubic or supercell geometries described in the previous section, with a lattice parameter of 3.95 Å. A 10×10×10 k-point sampling in Γ-centered cubic cells was used. The number of k-points was decreased proportionally as the number of cells increased in the supercell. The method of Methfessel-Paxton of order 1 was employed with a smearing value of 0.2. When atomic positions were fully relaxed residual forces were lower than 0.02 eV/Å.

The calculations presented here consider ferromagnetic ground states, because the small unit cell size enables a clear interpretation of the band structure. To analyze the band structures we fit the bands using maximally localized Wannier function[14] methods. Wannier functions were obtained using the Wannier90 code[34] provided by the VASP package to project the VASP bands onto localized orbitals. We chose an energy window encompassing the p-d band complex and projected the Bloch functions onto p-symmetry orbitals centered on the O sites and d-symmetry orbitals centered on the transition metal sites then minimized the MLWF spread. The resulting Wannier bands were in excellent agreement with the VASP bands. From the Wannier fits we then obtained on-site energies for the transition metal d and oxygen p levels, as well as d-p hopping amplitudes.

We determined the charge transfer by comparing the integral of the valence band charge density (from the VASP output file CHGCAR) over the volume of each cubic sub-cell of the heterostructure to the corresponding values obtained from obtained on the individual LMO and LNO cells in the cubic and rocksalt structures.

IV. RESULTS: ENERGY BANDS AND DENSITY OF STATES

The four panels of Figure 2 show the majority-spin energy bands of cubic $LaMnO_3$, cubic $LaNiO_3$,the 1/1 (001) superlattice and the rocksalt (double perovskite) La_2MnNiO_6.

Cubic $LaMnO_3$ is found to be metallic (obtaining insulating behavior requires including both the Jahn-Teller distortion and octahedral rotations). The bands that cross the fermi level are about 4 eV wide and are of primarily Mn e_g origin (hybridized with $O_{p\sigma}$ orbitals lying about 2eV below the Fermi level). These bands contain one electron shared between the two orbitals. In $LaNiO_3$ a similar situation occurs, but the rare earth perovskite nickelates are "negative charge transfer materials" in which the $O_{2p\sigma}$ orbitals lie in fact at a slightly higher energy than the Ni e_g orbitals implying, as will

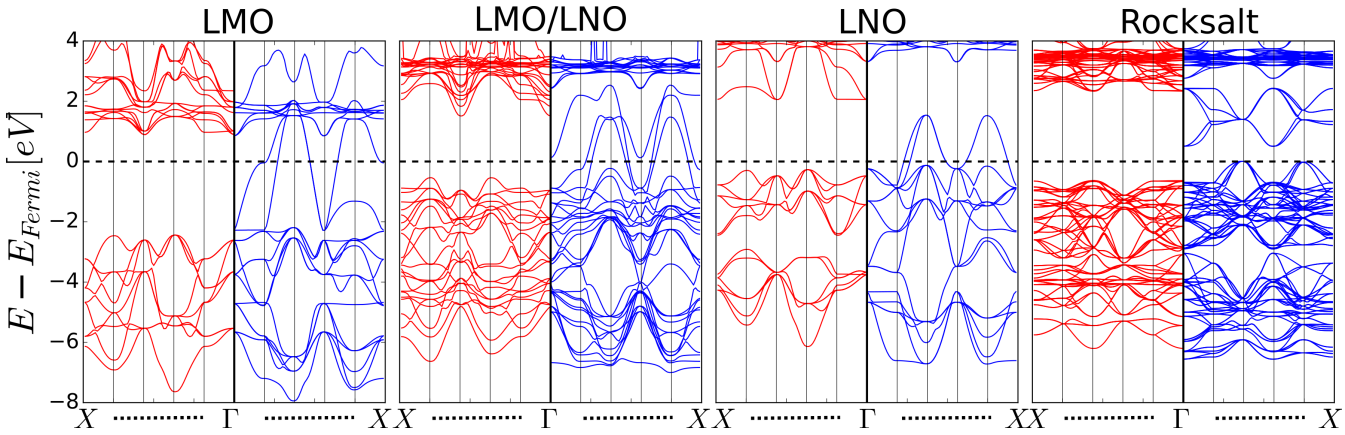

FIG. 2. Minority (left sub-panels) and majority spin (right sub-panels) bands of cubic $LaMnO_3$, $LaNiO_3$, the (001) $(LaNiO_3)_1/(LaMnO_3)_1$ superlattice and the rocksalt (111) La_2MnNiO_6 double perovskite. All calculations are performed for ferromagnetic ground states using the GGA+U method as described in the text. The bands are plotted along the high-symmetry lines $\Gamma \to X \to R \to \Gamma \to M \to X$ of the Brillouin zone.

be seen in more detail below, that the bands crossing the Fermi level are p-d e_g-symmetry hybrids with majority p character. The calculated band structure for the superlattice reveals a metallic state with two relatively wide bands that cross the Fermi level. As will be seen in more detail below, one of these bands arises from the Mn $d_{x^2-y^2}$ e_g state and the other from the Ni p-d hybrid state of the same symmetry. Also visible just above the fermi level is an unoccupied band mainly derived from the Mn-Ni antibonding combination of $d_{3z^2-r^2}$ e_g symmetry states (the bonding combination lies several eV below the Fermi level and is obscured by the many other orbitals in this energy range).

The metallic behavior of the superlattice may be understood as arising because the in-plane bands are only weakly affected by the superlattice formation. The wide energy range over which the bands disperse inhibits complete charge transfer. In fact, the net charge transferred from the Mn plane to the Ni plane is 0.4 e/unit cell. The calculated bands for the rocksalt structure reveal an insulator, essentially because in this structure both e_g orbitals on the Mn site mix strongly with the e_g orbitals on the Ni site, allowing splitting of all bands. The narrower bandwidth also promotes a larger charge transfer, approximately 0.7 e/unit cell.

To elucidate the physics revealed by our calculated band structures we consider the electronic density of states, projected onto given symmetry states of individual atoms. Fig. 3 shows the orbitally projected densities of states for the cubic parent materials. From the top two rows we see that in $LaMnO_3$ the near Fermi surface states are e_g symmetry antibonding d-p hybrids, with majority d character. The corresponding bonding states are visible as the peak centered at $\approx -7eV$. Comparison of the relative amplitude of bonding and antibonding states in the d and p partial DOS confirms that the e_g d-states lie above the p-states in this material. The t_{2g}-symmetry states are fully filled, and couple less strongly

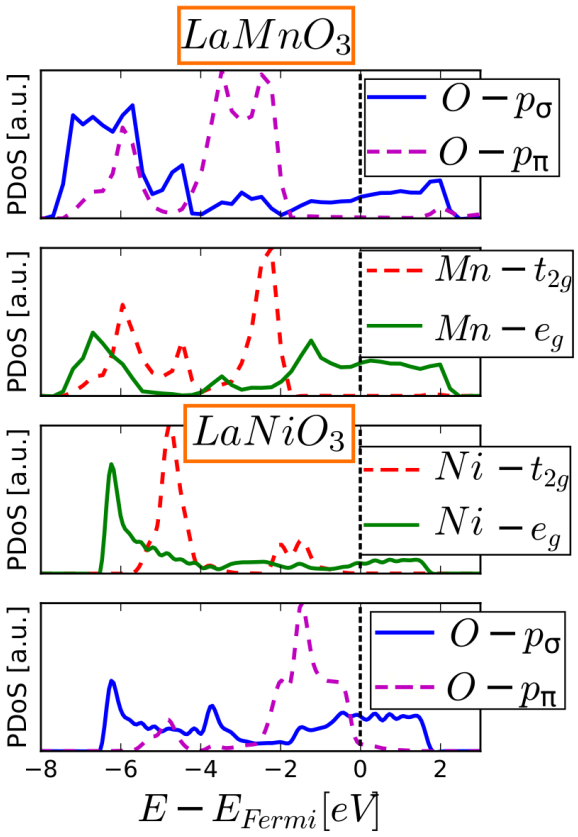

FIG. 3. Projection of the majority spin density of states of ferromagnetic cubic $LaMnO_3$ and $LaNiO_3$ onto the transition metal (Mn or Ni) d orbitals and onto oxygen p orbitals. The e_g-symmetry and t_{2g}-symmetry orbitals are plotted separately (color online) as are the oxygen p_σ (hybridizing with the transition metal e_g) and p_π (not hybridizing with the transition metal e_g orbitals).

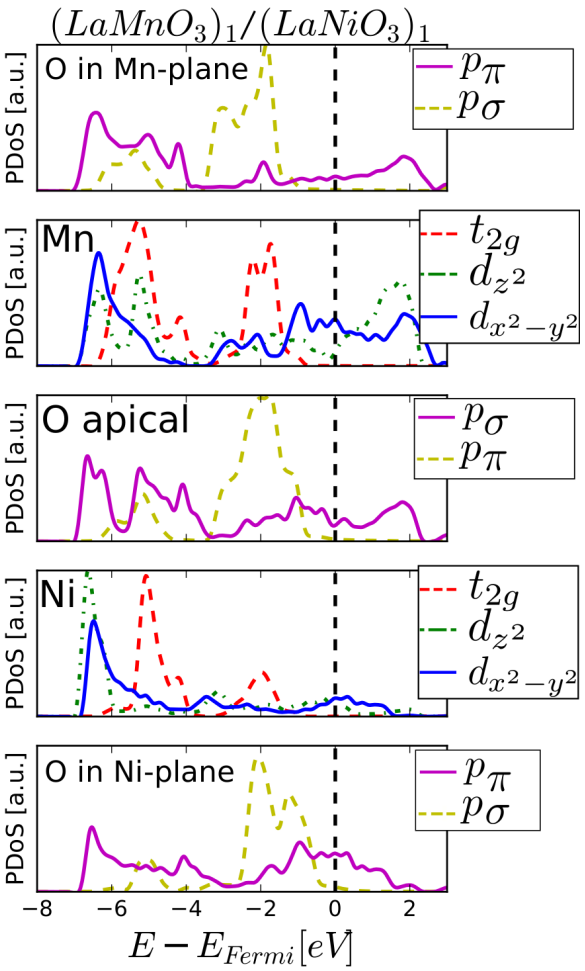

FIG. 4. Projection of the majority spin density of states of the ferromagnetic $(LaNiO_3)_1/(LaMnO_3)_1$ superlattice onto the transition metal (Mn or Ni) d orbitals and onto oxygen p orbitals. The two e_g orbitals are plotted separately, but all three t_{2g} orbitals are added up together. The oxygen p_σ (hybridizing with the transition metal e_g) and p_π (not hybridizing with the transition metal e_g orbitals) distinguished.

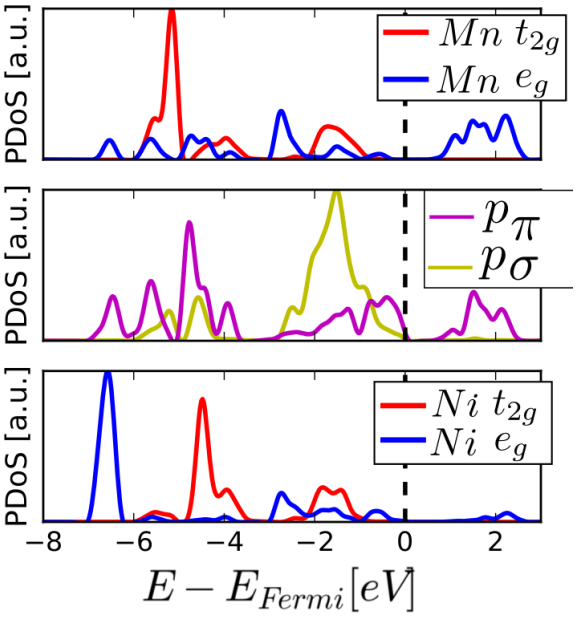

FIG. 5. Projection of the majority spin density of states of ferromagnetic rocksalt $A_2BB'O_6$ onto e_g and t_{2g} orbitals are plotted separately. The oxygen p_σ (hybridizing with the transition metal e_g) and p_π (not hybridizing with the transition metal e_g orbitals) distinguished.

to the oxygen orbitals, as revealed by their smaller peak width and smaller bonding-antibonding splitting.

Turning now to the lower two panels we see that for $LaNiO_3$ the Ni p-d manifold is somewhat narrower in energy than the p-d manifold in the Mn compound, reflecting a weaker p-d hybridization in the Ni material. We also see that most of the e_g-symmetry d density of states lies far below the fermi level indicates that in $LaNiO_3$ the material is in the 'negative charge transfer' class of materials in which the d-states lie lower than the oxygen states and are further pushed down by p-d hybridization, as expected from the greater electronegativity of Ni relative to Mn and amply documented in the literature. As in the Mn compound the Ni t_{2g} states are fully filled and rather less strongly hybridized to the oxygen than the e_g states.

We now turn to the density of states of the superlattice, shown in Fig. 4. The top panel shows the density of states projected onto the oxygen states lying in the $Mn - O$ plane, and the second panel shows the DOS projected onto the Mn states. Comparison to the corresponding panels of Fig. 3 shows that the superlattice-induced changes to the Mn-plane O orbitals and the Mn $d_{x^2-y^2}$ orbital are negligible. A splitting of the Mn $d_{3z^2-r^2}$ orbital is evident (leading e.g. to the suppressed DOS at the Fermi level) with corresponding shifts to the "apical" (in-between Mn and Ni planes) oxygen orbital. Similarly, examination of the projection of the density of states onto the Ni and Ni-plane O orbitals reveals negligible changes to the planar orbitals; the small weight of the Ni d orbitals near the fermi level makes changes in the Ni $d_{3z^2-r^2}$ orbitals difficult to discern + These results confirm that one of the bands that crosses the Fermi level is primarily of Mn $d_{x^2-y^2}$ character and the other primarily of O character but within the $Ni - O$ plane, with the antibonding portion of the Mn $d_{3z^2-r^2}$ orbital and the O_{p_z} orbital split, with one portion pushed up in energy above the Fermi level by backscattering associated with the breaking of translational symmetry in the superlattice.

Finally, in Fig. 5 we show the partial densities of states for the rocksalt structure. The Mn d orbitals are now to a large degree pushed up above the Fermi level and the Ni d orbitals and oxygen orbitals are submerged below, leading to insulating behavior and a larger degree of charge transfer.

V. PARAMETER TRANSFERABILITY: WANNIER ANALYSIS

The panels of Fig. 2 show that as the unit cell becomes larger, the number of energy bands increases, as does the band overlap, so the physics becomes more difficult to analyse. The bands would become even more complicated if octahedral rotations or antiferromagnetism were considered. For this reason, an important issue in analysing the physics of nontrivial situations is parameter 'transferability': specifically, whether one can use parameters obtained in simpler situations to model more complicated ones. We have examined the transferability issue in the systems we consider by performing a Maximally Localized Wannier Function (MLWF) analysis of our calculated bands for each of the structures. The MLWF analysis can be thought of as an unbiassed determination of tight-binding parameters; comparison of the parameters obtained for different situations then provides an estimate of transferability.

We find that the hopping amplitudes (inter-orbital matrix elements of the DFT+U Hamiltonian) between Mn or Ni and the co-planar O are the same within a few percent for all structures (e.g. the Mn e_g-O2p_σ hopping is 1.7 and the Ni e_g-O2p_σ hopping is 1.3eV). We conclude that the hopping parameters are transferable.

The on-site energies (orbital-diagonal matrix elements of the DFT+U Hamiltonian) exhibit variation among systems. One contribution to the variation is changes to the combination of Madelung energies associated with different chemical environments as well as any electric fields arising from charge transfer (this is essentially the intrinsic contribution to the work function difference that gives rise to band-bending at interfaces). For example, the photoemission data reported by Yoshimatsu et al for $SrVO_3/SrTiO_3$ quantum wells[11,12], indicates a $\sim 0.9eV$ shift in the oxygen energy from the one material to the other. A second contribution to the variation is a change of physics, in particular a variation of the p-d energy level splitting, which plays a crucial role in the physics of transition metal oxides[35,36].

TABLE I. Orbital energies obtained from Maximally Localized Wannier analysis for majority spin band structures computed with $U_{Mn} = 4$, $U_{Ni} = 6$ eV. $J = 1eV$ and measured relative to the Fermi level.

Orbital	$LaMnO_3$	SL	RS	$LaNiO_3$
Mn_{z^2}	-2.2	-1.7	-1.1	–
$Mn_{x^2-y^2}$	-2.2	-2.0	-1.4	–
O:Mn-plane	-4.6	-3.8	-2.3	–
O:Apical	-4.6	-3.4	-3.0	-2.8
Ni_{z^2}	–	-4.2	-4.0	1.6
$Ni_{x^2-y^2}$	–	-3.9	-4.0	1.6
O:Ni-plane	–	-3.0	-2.3	-2.8

TABLE II. Orbital energies obtained from Maximally Localized Wannier analysis for minority spin band structures computed with $U_{Mn} = 4$, $U_{Ni} = 6$ eV. $J = 1eV$ and measured relative to the Fermi level.

Orbital	$LaMnO_3$	SL	RS	$LaNiO_3$
Mn_{z^2}	-0.8	2.3	1.2	–
$Mn_{x^2-y^2}$	-0.8	2.6	1.2	–
O:Mn-plane	-3.6	-4.1	-2.2	-
O:Apical	-3.6	-4.5	-3.2	-2.8
Ni_{z^2}	–	1.3	3.4	1.6
$Ni_{x^2-y^2}$	–	1.6	4.4	1.6
O:Ni-plane	–	-3.0	-3.1	-2.8

Table I presents the energies of the Mn and Ni e_g symmetry orbitals as well as the energies of the p_σ orbitals on different oxygen sites, distinguishing (for the layered structure) between oxygen states in the Mn or Ni plane and the apical oxygen sites that bridge the Mn and Ni planes. The 'band-bending' or work function differences are clearly visible as differences between the energy of the O in the MnO_2 and NiO_2 planes. In addition, a change in the relative energies of the oxygen p and transition metal d levels is apparent.

For cubic $LaMnO_3$ we have $E^{Mn}_{e_g} - E^{O}_{2p\sigma} \approx 2.4$eV while for $LaNiO_3$ we find $E^{Ni}_{e_g} - E^{O}_{2p\sigma} \approx$ -0.9 eV, reflecting the negative charge transfer nature of the Ni compound. In the rocksalt structure we find $E^{Mn}_{e_g} - E^{O}_{2p\sigma} \approx$ 1.6 eV, about 0.6eV *less* than in bulk $LaMnO_3$ while $E^{Ni}_{e_g} - E^{O}_{2p\sigma} \approx$ -1.0 eV, essentially unchanged from bulk $LaNiO_3$. In the superlattice we see that the energy difference between the average of the energies of the two Mn orbitals and the energy of the in-plane oxygen σ orbital $E^{Mn}_{e_g} - E^{O}_{2p\sigma} \approx 2.0$ eV. We thus conclude that the charge transfer energy is *not* transferable. The fact that the change is larger in the rocksalt than in the superlattice structure suggests that the d-valence makes an important contribution to the p-d level splitting.

Interestingly the p-d splitting on Ni site is almost material independent. We attribute this to the negative charge transfer nature of the material, which implies (as can be seen from the density of states plot) that the near Fermi surface states are of primarily oxygen character. Thus in the approximation used here the actual charge density on the Ni sites changes only slightly (loosely speaking the Ni-O plane goes from $d^8\bar{L}$ to d^8 as charges are added) and the mean valence of each of the 3 oxygens changes by less than e/3, so the oxygen Hartree shift is minimal, explaining why the $\varepsilon_d - \varepsilon_p$ changes only slightly.

Zhong and Hansmann[15] studied the dependence of the key $\varepsilon_d - \varepsilon_p$ parameter on charge transfer, focussing on compounds involving early and middle transition metal oxides. Their observation that the ionization/affinity energies of transition metal ions depend on the occupancy and thus affect band offsets and charge transfer is impor-

tant. However our results indicate that the statements in Ref.[15] that the p-d splitting scales with the product of the on-site U and charge transfer is not always correct. We find clear differences between the shifts on the Mn layer and the Ni layer, presumably related to the negative charge transfer nature of perovskite nickel oxide. Further, we find, in agreement with previous literature,[36] that the double counting correction to a large degree eliminates the Hartree shift so within the formalism used here the connection between charge transfer, p-d splitting and U cannot be as simple as that proposed by Zhong et. al. Perhaps for this reason Eq. 3 of Ref. 15 relating the shift of p-level energies to charge transfer is not consistent with the data in Table I either for the Mn site or the Ni site. As a more minor point we note that different d-level states and different oxygen ions behave differently: restricting attention to "the [presumably orbitally averaged] d-level energy" and "oxygen energy" may gloss over important physics.

VI. COMPARISON TO EXPERIMENT

The essential features of the experiment of Hoffman et al[13] are that for $(LaMnO_3)_n/(LaNiO_3)_n$ superlattices with $n \leq 2$ the ground state was insulating and an almost complete charge transfer of one electron occurred from the Mn to the Ni. These behaviors are not reproduced by the calculations, which predict that even for the $n = 1$ superlattice we have metallic behavior with $\sim 0.4e$ charge transfer. The two effects are closely related: the planar orbitals ($d_{x^2-y^2}$ and in-plane p_σ) are only minimally affected by superlattice formation, and the resulting bandwidths are so large that the moderate Mn-Ni electronegativity difference cannot empty out the Mn d-bands. While our calculations are based on the DFT+U approximation, a Hartree approximation to a complicated many-body situation, we believe that correcting the deficiencies of this approximation are unlikely to change the basic theoretical prediction because the conclusion arises from eV-scale energetics of different valence states, which are well captured by DFT/Hartree approximations.

The results presented here were derived from idealized cubic-type structures, however we have also investigated the consequences of changing the structure. Changing the lattice parameter of the cells to those of LNO or LMO only changes the dispersion of the electronic states. Modifying the spin orientation on the Mn and Ni sites to the anti-ferromagnetic coupling does not open a full band gap in any of the heterostructures considered: the $d_{x^2-y^2}$ band remains metallic in all cases. For the model (1,1) superlattice presented in the previous section, all internal coordinates were fully relaxed with VASP, keeping the unit cell parameters fixed. The initial condition was taken to be the ideal tetragonal structure cell. In the relaxed structures all forces were less than 1 meV/Å. The physics of the relaxed structures was not materially different from the physics of the unrelaxed structures with moderate charge transfer and wide metallic bands derived from the e_g orbitals crossing the Fermi level.

Another possibility is that the electron transfer and differing hybridization strengths will cause motion of the apical oxygen away from the Ni and towards the Mn. However relaxing the internal coordinates only leads to a $\sim 0.1\mathring{A}$ shift in the apical O position, too small to change the energetics significantly. We also investigated variant structures in which the apical O is displaced by 0.2Å and $0.4\mathring{A}$ toward the Mn. The charge transfer increases to 0.53 and 0.7 electrons respectively, but the $d_{x^2-y^2}$-derived orbitals remain partially occupied and the superlattice remains metallic.

Interestingly, the rocksalt structure has a similar $0.7e$ charge transfer, but is insulating, essentially because the backscattering associated with the Mn-Ni alternation opens a band gap. We conclude that the insulating behavior requires disruption of the in-plane Mn-O and Ni-O networks and speculate that a high density of Mn/Ni atisite defects in the near interface layers could disrupt the in-plane networks as well as promoting larger charge transfer, thus producing physics similar to that found in the calculations of the rocksalt structure. In this regard it is interesting to note that evidence of substantial Ni-Mn intermixing, especially for the near-substrate layers, has been very recently reported in a closely related superlattice.[37]

Finally we consider the $(LaNiO_3)_2/(LaMnO_3)_2$ superlattice with a 2×2×4 computational unit cell, which allows for two sublattice charge and Jahn-Teller order on the Mn and Ni layers. All internal degrees of freedom were fully relaxed with VASP until forces were less than 1 meV/Å. We started from two initial conditions: the pseudo-cubic structure considered above, and a structure in which the LMO has the bulk LMO two sublattice Jahn-Teller order and the LNO has no order. For both sets of initial conditions and all U-values, we find that there are also modest octahedral rotations and a weak tow-sublattice Jahn-Teller-like structural distortion, but the hybrid structure remains metallic with numerous bands crossing the Fermi level. A projected DOS analysis (see Figure 6c and d) demonstrates that in this structure the metallic behavior arises primarily from the wide $d_{x^2-y^2}$ bands of both the Mn and Ni sublattices.

Other attempts to reproduce the experimental band gap starting with different geometries and +U values were also conducted. Two different sets of +U parameters were considered: $U_{Mn} = 2$, $U_{Ni} = 4$, and $U_{Mn} = 8$, $U_{Ni} = 6$. In both cases, a 2× 2 × 2 cubic supercell of LNO was placed on the top of an already relaxed 2× 2 × 2 supercell of LMO with appropriate Jahn-Teller distortions yielding a metallic band diagram. Geometries were allowed to fully relax, leading to final structures rather similar to the one in Figure6 for both sets of +U parameters. In both cases the LNO sublattice followed the distortion of the LMO, which in turn did not change to a cubic geometry, as reported in experiments. Energy

band diagrams displayed in Figure8 of the Appendix.

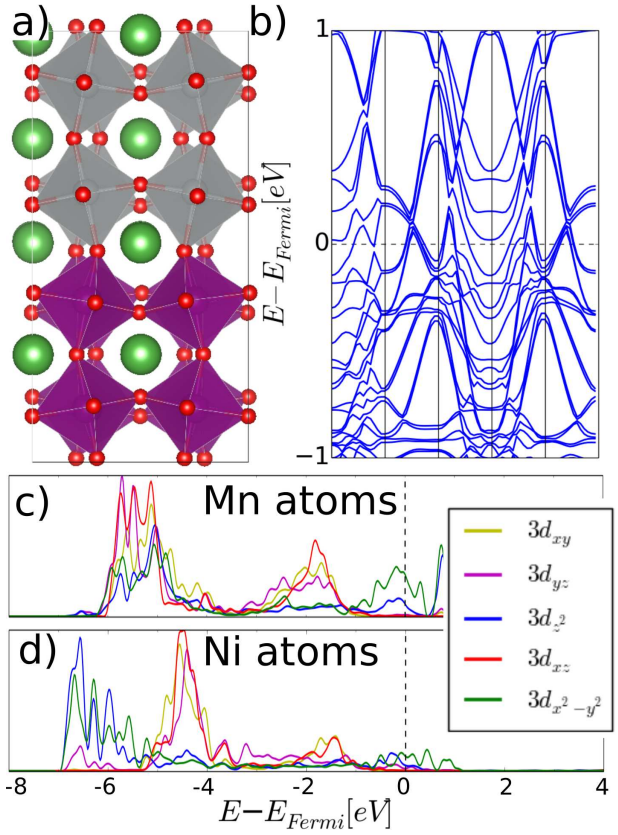

FIG. 6. a) Schematic representation of the relaxed cubic $(LaNiO_3)_2/(LaMnO_3)_2$ heterostructure. b) Band structure of the majority spin. The projected DoS (PDoS) onto the d orbitals of the two types of nonequivalent Mn atoms is plotted in c) and d).The bands are plotted along the high-symmetry lines $\Gamma \to X \to R \to \Gamma \to M \to X$ of the Brillouin zone.

VII. CONCLUSIONS

First-principles calculations of model $LaMnO_3$ and $LaNiO_3$ structures reveal that the basic physics of the superlattice situation is controlled by geometry, which determines hopping amplitudes and thus band structures, and by relative electronegativity of the transition metal ions, which determines charge transfer. Our calculations strongly suggest that in the ideal superlattice, the wide $d_{x^2-y^2}$ symmetry bands are essentially unaffected by superlattice formation and remain metallic because the Mn-Ni electronegativity difference is smaller than the bandwidth, so the Mn-derived bands remain partly occupied and the Ni-derived bands remain partly empty. This should be contrasted to $LaTiO_3/LaNiO_3$ superlattices studied previously. Theoretical calculations predict[38] and experiment confirms[39] that in $LaNiO_3/LaTiO_3$ superlattices, one electron is transferred from the $LaTiO_3$ layer to the $LaNiO_3$ layer, hanging the formal valence to a configuration similar to that of rocksalt NiO, a well known Mott/charge transfer insulator and producing insulating behavior. In this system this happens because the Ti-Ni electronegativity difference is large enough and the Ti d_{xy} band is narrow enough that nearly complete charge transfer occurs. We also note the $SrVO_3/SrTiO_3$ superlattices modelled by by Zhong et al.[10] where there is essentially no charge transfer and the physics is of dimensionality reduction and confining potentials.

An analysis based on maximally localized Wannier functions demonstrates that transition metal/oxygen hybridization amplitudes and oxygen site energies are "transferable", so that parameters derived from calculations performed in simple geometries can be used in phenomenological models of more complex situations. However, the transition metal d-oxygen p level splitting is not transferable: it is found to depend on the charge transfer, essentially because the transition metal electronegativity depends on d-occupancy.

For the LMO/LNO system that motivated our study, we found that within our theoretical framework the only viable explanation for the observed insulating behavior of thin superlattices was a large concentration of antisite defects, essentially because of the partial charge transfer leading to partial filling of the relatively wide planar (x^2-y^2-derived) bands. Note that our structural relaxations indicate that octahedral reotations are far from being large enough to narrow the bands and eliminate band overlap. Some experimental evidence for antisite defects has recently been reported[37]. As a possible alternative, we note that it is conceivable that some other mechanism (e.g. thermal fluctuations at higher temperatures) might lead to octahedral rotations of much larger amplitude than considered here, perhaps reducing the bandwidth in the layered structures enough to eliminate the overlap between bands, thereby allowing a larger charge transfer leading to insulating behavior. Experimental investigation of antisite defects and of octahedral rotations would be valuable.

We suggest directions for future theoretical research. First, the charge transfer depends on the difference in electronegativity as also noted by Zhong and Hansmann[15] (although as explained above the details of our findings are not in complete agreement with theirs). The DFT+U approach used here provides an approximation to the electronegativity difference. The issue also relates to basic questions of the double counting in the '+U' methodology. Further studies of these issues by other methods would be valuable. Second, here parameter transferability has been investigated in one particular material system. We conjecture that the main result (transfer of all parameters except for the p-d level splitting) will extend to all transition metal oxides heterostructures, but further investigation would be desirable. Perhaps most importantly, it appears from our results that the difference between the energies of the p and d orbitals of the Mn cation is not transferable between structures and that change in the p-d splitting in late transition metal oxides (e.g. the Ni compound we stud-

ied) may be different than in the early transition metal ions.

VIII. ACKNOWLEDGMENTS

This work was supported by the U.S. Department of Energy, Office of Science, Basic Energy Sciences, Materials Science and Engineering Division. We acknowledge the computing resources provided on Blues and Fusion, the high-performance computing clusters operated by the Laboratory Computing Resource Center at Argonne National Laboratory.

* alejandrolb@gmail.com

[1] J. Chakhalian, J. W. Freeland, A. J. Millis, C. Panagopolous, and J. M. Rondinelli, Rev. Mod. Phys. **86**, 1189 (2014).
[2] M. Imada, A. Fujimori, and Y. Tokura, Rev. Mod. Phys. **70**, 1039 (1998).
[3] Y. Tokura, Rep. Prog. Phys. **69**, 797 (2006).
[4] T. Kimura and Y. Tokura, Annual Review of Materials Science **30**, 451 (2000).
[5] S. Middey, J. Chakhalian, P. Mahadevan, J. Freeland, A. Millis, and D. Sarma, Annual Review of Materials Research **46**, 305 (2016).
[6] M. Gibert, P. Zubko, R. Scherwitzl, J. Iniguez, and J.-M. Triscone, Nature Materials **11**, 195 (2012).
[7] C. Piamonteze, M. Gibert, J. Heidler, J. Dreiser, S. Rusponi, H. Brune, J.-M. Triscone, F. Nolting, and U. Staub, Phys. Rev. B **92**, 014426 (2015).
[8] J. D. Hoffman, B. J. Kirby, J. Kwon, G. Fabbris, D. Meyers, J. W. Freeland, I. Martin, O. G. Heinonen, P. Steadman, H. Zhou, C. M. Schlepütz, M. P. M. Dean, S. G. E. te Velthuis, J.-M. Zuo, and A. Bhattacharya, Phys. Rev. X **6**, 041038 (2016).
[9] A. T. Lee and M. J. Han, Phys. Rev. B **88**, 035126 (2013).
[10] Z. Zhong, Q. Zhang, and K. Held, Phys. Rev. B **88**, 125401 (2013).
[11] K. Yoshimatsu, T. Okabe, H. Kumigashira, S. Okamoto, S. Aizaki, A. Fujimori, and M. Oshima, Phys. Rev. Lett. **104**, 147601 (2010).
[12] K. Yoshimatsu, K. Horiba, H. Kumigashira, T. Yoshida, A. Fujimori, and M. Oshima, Science **333**, 319 (2011).
[13] J. Hoffman, I. C. Tung, B. B. Nelson-Cheeseman, M. Liu, J. W. Freeland, and A. Bhattacharya, Phys. Rev. B **88**, 144411 (2013).
[14] N. Marzari and D. Vanderbilt, Phys. Rev. B **56**, 12847 (1997).
[15] Z. Zhong and P. Hansmann, Phys. Rev. X **7**, 011023 (2017).
[16] H. Chen and A. Millis, Phys. Rev. B **93**, 104111 (2016).
[17] T. Mizokawa, D. I. Khomskii, and G. A. Sawatzky, Phys. Rev. B **61**, 11263 (2000).
[18] M. J. Han, X. Wang, C. A. Marianetti, and A. J. Millis, Phys. Rev. Lett. **107**, 206804 (2011).
[19] H. Park, A. J. Millis, and C. A. Marianetti, Phys. Rev. Lett. **109**, 156402 (2012).
[20] S. Johnston, A. Mukherjee, I. Elfimov, M. Berciu, and G. A. Sawatzky, Phys. Rev. Lett. **112**, 106404 (2014).
[21] P. W. Anderson and H. Hasegawa, Phys. Rev. **100**, 675 (1955).
[22] A. J. Millis, P. B. Littlewood, and B. I. Shraiman, Phys. Rev. Lett. **74**, 5144 (1995).
[23] J. Kanamori, J. Appl. Phys. **31**, 14S (1960).
[24] J. B. A. A. Ellemans, B. van Laar, K. R. van der Veen, and B. O. Loopstra, J. Solid State Chem. **3**, 238 (1971).
[25] A. M. Zhang, S. L. Cheng, J. G. Lin, and X. S. Wu, J. Appl. Phys. **117**, 17B325 (2015).
[26] C. Franchini, R. Kováčik, M. Marsman, S. S. Murthy, J. He, C. Ederer, and G. Kresse, Journal of Physics: Condensed Matter **24**, 235602 (2012).
[27] E. A. Nowadnick, J. P. Ruf, H. Park, P. D. C. King, D. G. Schlom, K. M. Shen, and A. J. Millis, Phys. Rev. B **92**, 245109 (2015).
[28] P. E. Blöchl, Phys. Rev. B **50**, 17953 (1994).
[29] J. P. Perdew, K. Burke, and M. Ernzerhof, Phys. Rev. Lett. **77**, 3865 (1996).
[30] S. L. Dudarev, G. A. Botton, S. Y. Savrasov, C. J. Humphreys, and A. P. Sutton, Phys. Rev. B **57**, 1505 (1998).
[31] G. Kresse and J. Hafner, Phys. Rev. B **48**, 13115 (1993).
[32] G. Kresse and J. Furthmüller, Phys. Rev. B **54**, 11169 (1996).
[33] G. Kresse and D. Joubert, Phys. Rev. B **59**, 1758 (1999).
[34] A. A. Mostofi, J. R. Yates, Y.-S. Lee, I. Souza, D. Vanderbilt, and N. Marzari, Computer Physics Communications **178**, 685 (2008).
[35] J. Zaanen, G. A. Sawatzky, and J. W. Allen, Phys. Rev. Lett. **55**, 418 (1985).
[36] H. T. Dang, A. J. Millis, and C. A. Marianetti, Phys. Rev. B **89**, 161113 (2014).
[37] J.-H. Kwon, J. HOrrman, R. Yuan, A. Yoon, A. Bhattacharya, and J.-M. Zuo, Semicond. Scie. Technol. **32**, 014002 (2017).
[38] H. Chen, A. J. Millis, and C. A. Marianetti, Phys. Rev. Lett. **111**, 116403 (2013).
[39] Y. Cao, Z. Yang, M. Kareev, X. Liu, D. Meyers, S. Middey, D. Choudhury, P. Shafer, J. Guo, J. W. Freeland, E. Arenholz, L. Gu, and J. Chakhalian, Phys. Rev. Lett. **116**, 076802 (2016).

IX. APPENDIX: WANNIER ANALYSIS

To obtain model Hamiltonians we resort to the the maximally localized Wannier functions (MLWFs)[14], obtained using the Wannier90 code[34] from the first-principles ground state obtained with VASP. By projecting onto p and d orbitals and minimizing the MLWF spread, the band structure obtained using the first-principles approach compared to the Wannier interpolation were in excellent agreement. Fig. 7 shows a comparison for the 4 structures of interest.

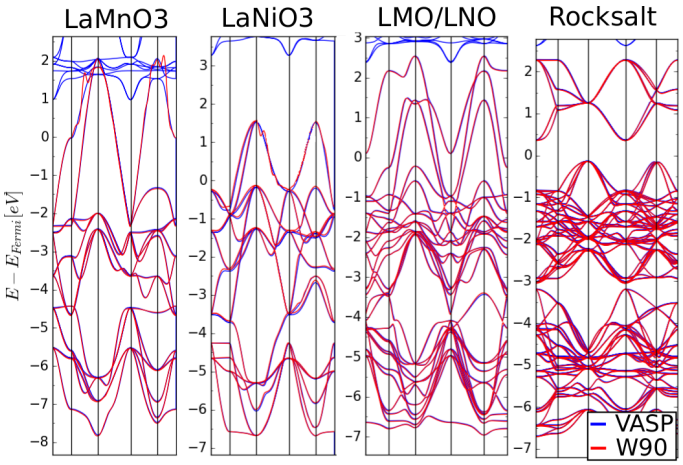

FIG. 7. Comparison of the first-principles obtained band structure with the Wannier90 interpolated band structure for cubic $LaMnO_3$, cubic $LaNiO_3$, $(LaNiO_3)_1/(LaMnO_3)_1$ heterostructure, and ferromagnetic rocksalt.

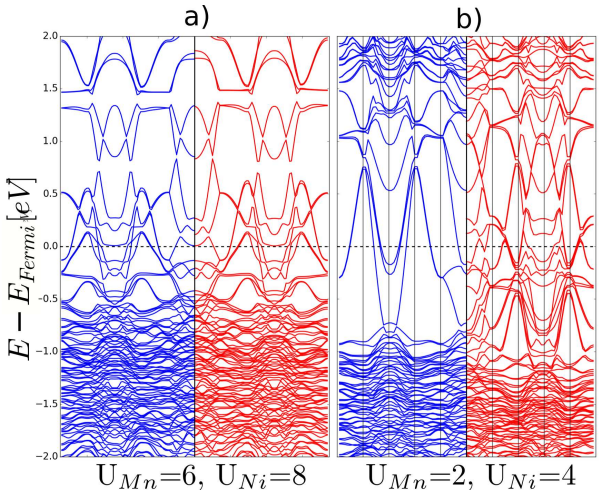

FIG. 8. Minority (left sub-panels) and majority spin (right sub-panels) bands of $2 \times 2 \times 4$ $(LaNiO_3)_2/(LaMnO_3)_2$ heterostructure for different sets of +U values (J=1). a) $U_{Mn} = 6$, $U_{Ni} = 8$, $U_{Mn} = 2$, $U_{Ni} = 4$. The bands are plotted along the high-symmetry lines $\Gamma \to X \to R \to \Gamma \to M \to X$ of the Brillouin zone.